FR Cnc Revisited: Photometry, Polarimetry and Spectroscopy*

A. Golovin[1]†, M.C. Gálvez-Ortiz[2,3], M. Hernán-Obispo[4], M. Andreev[1,5,6],
J.R. Barnes[3], D. Montes[4], E. Pavlenko[7], J.C. Pandey[8], R. Martínez-Arnáiz[4],
B.J. Medhi[8], P.S. Parihar[9], A. Henden[10], A. Sergeev[5,6], S.V. Zaitsev[1], N. Karpov[5,6]

[1] *Main Astronomical Observatory of National Academy of Sciences of Ukraine, Zabolotnogo str., 27, Kiev, 03680, Ukraine*
[2] *Centro de Astrobiología (CSIC-INTA). Crta, Ajalvil km 4. E-28850 Torrejón de Ardoz, Madrid, Spain*
[3] *Centre for Astrophysics Research, University of Hertfordshire, College Lane, Hatfield, Hertfordshire AL10 9AB, UK*
[4] *Astrophysics department, Physic Faculty, Universidad Complutense de Madrid, E-28040 Madrid, Spain*
[5] *Terskol Branch of the Astronomy Institute of RAS, Kabardino-Balkaria Republic, 361605, Russia*
[6] *International Center for Astronomical, Medical and Ecological Research of National Academy of*
Sciences of Ukraine (ICAMER of NASU), Zabolotnogo str., 27, Kiev, 03680, Ukraine
[7] *Crimean Astrophysical Observatory (CrAO), Nauchny, 98409, Ukraine*
[8] *Aryabhatta Research Institute of Observational Sciences (ARIES), Manora Peak, Nainital, 263129, India*
[9] *Indian Institute of Astrophysics, Block II, Koramangala, Bangalore, 560 034, India*
[10] *AAVSO, Clinton B. Ford Astronomical Data and Research Center, 49 Bay State Rd. Cambridge, MA 02138, USA*

ABSTRACT

This is a part of a multiwavelength study aimed at use of complementary photometric, polarimetric and spectroscopic data to achieve an understanding of the activity process in late-type stars. Here we present the study of FR Cnc, a young, active and spotted star.

We performed analysis of $ASAS-3$ (The All Sky Automated Survey) data for the years 2002–2008 and amended the value of the rotational period to be 0.826518 d. The amplitude of photometric variations decreased abruptly in the year 2005, while the mean brightness remained the same, which was interpreted as a quick redistribution of spots. BVR_c and I_c broad band photometric calibration was performed for 166 stars in FR Cnc vicinity.

The photometry at Terskol Observatory shows two brightening episodes, one of which occurred at the same phase as the flare of 2006 November 23. Polarimetric BVR observations indicate the probable presence of a supplementary source of polarization. We monitored FR Cnc spectroscopically during the years 2004–2008. We concluded that the RV changes cannot be explained by the binary nature of FR Cnc. We determined the spectral type of FR Cnc as K7V. Calculated galactic space-velocity components (U, V, W) indicate that FR Cnc belongs to the young disc population and might also belong to the IC 2391 moving group. Based on Li I $\lambda6707.8$ measurement, we estimated the age of FR Cnc to be between 10–120 Myr. Doppler Tomography was applied to create a starspot image of FR Cnc. We optimized the goodness of fit to the deconvolved profiles for axial inclination, equivalent width and $v \sin i$, finding $v \sin i = 46.2$ km s^{-1} and $i = 55°$. We also generated a synthetic V-band lightcurve based on Doppler imaging that makes simultaneous use of spectroscopic and photometric data. This synthetic lightcurve displays the same morphology and amplitude as the observed one.

The starspot distribution of FR Cnc is also of interest since it is one of the latest spectral types to have been imaged. No polar spot was detected on FR Cnc.

Key words: stars: activity – stars: flare – stars: rotation – stars: individual: FR Cnc.

arXiv:1111.6595v2 [astro-ph.SR] 30 Nov 2011

1   INTRODUCTION

It is well-known that late-type stars show magnetic activity similar to the activity of our Sun, but the physics of 'stellar' activity is not yet well understood. In addition, the activity level manifested by late-type stars is much higher than that observed for the Sun.

FR Cnc (= BD+16 1753 = MCC 527 = 1ES 0829+15.9 = 1RXS J083230.9+154940 = HIP 41889) was first mentioned as a probable active star when it was identified as the optical counterpart of a soft X-ray source 1ES 0829+15.9 in the *Einstein Slew Survey*. It has V = 10.43 mag, spectral type K8V, the X-ray flux of $\approx 10^{-11}$ erg s^{-1} cm^{-2} (Elvis et al. 1992; Schachter et al. 1996). Lately, this object was rediscovered as an X-ray source 1RXS J083230.9+154940 in the *ROSAT* All-Sky Survey (RASS) with lower X-ray flux at the level of 2×10^{-12} erg s^{-1} cm^{-2} (Voges et al. 1999). The X-ray luminosity of $(2 - 12) \times 10^{29}$ erg s^{-1} and the ratio of X-ray to bolometric luminosity $\frac{F_x}{F_{bol}}$ of $\geqslant 10^{-3.3}$ (Pandey et al. 2005) indicates that this object has an active corona (Schachter et al. 1996).

In the *Hipparcos* catalogue this star was mentioned as an unsolved variable star with the identifier HIP 41889 and 0.17 mag amplitude of variability (Perryman et al. 1997). It was classified as BY Dra type star (i.e. its variability caused by rotational modulation of starspots) and given the name FR Cnc by Kazarovets et al. (1999). For analysis of *Hipparcos* observations see Pandey et al. (2005). FR Cnc (RA(2000) = $08^h32^m30\overset{s}{.}5287$ and Dec. (2000) = $+15°49'26\overset{''}{.}193$) has 30.24 $\pm$ 2.03 marcsec parallax (Perryman et al. 1997) that implies a distance of 33 $\pm$ 2 pc and an absolute magnitude of 7.8. The kinematics of FR Cnc suggests that it is a very young (35–55 Myr) main-sequence star and a possible member of the IC 2391 supercluster, as it was shown by Pandey et al. (2005). Upgren et al. (2002) concluded that FR Cnc is not a binary system, based on two measurements of the RV.

The presence of Ca II H & K and Hα emission lines in the spectra indicates high chromospheric activity in FR Cnc (Pandey et al. 2002; Pandey 2003). In 'quiescent' state this
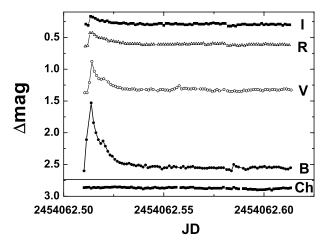
Figure 1. Lightcurve of FR Cnc on 2006 November 23 from Golovin et al. (2007): "The flare of FR Cnc: shifted differential lightcurves in $B-$, $V-$, $R-$ and $I-$bands as well as the difference *check star − comparison star* ('Ch' on the plot)"

object manifests optical variability with the dominant period 0.8267 $\pm$ 0.0004 d due to the presence of starspots and axial rotation (Pandey et al. 2005). In addition, photometry obtained in 2005 February – April with Kilodegree Extremely Little Telescope indicates FR Cnc optical variability with 0.827 d period (Pepper et al. 2008) when monitoring the Praesepe open cluster for transiting exoplanets.

The first ever-detected optical flare of this object was observed during CCD photometry of FR Cnc on 2006 November 23 at Crimean Astrophysical Observatory (Ukraine) with 38-cm Cassegrain telescope and described by Golovin et al. (2007). The flare was observed in $BVRI$-bands (see Fig. 1). The amplitude reached even 1 mag in the B-band and was decreasing towards the I-band. The flare energy output in the B-band was about 1.73×10^{31}erg $\overset{\circ}{A}^{-1}$ and flare to quiescent flux ratio was 38.63 per cent.

2   PHOTOMETRIC OBSERVATIONS

Most of the information on the photospheric activity (e.g. starspots) of BY Dra-type stars comes from photometric observations. The mean brightness level is strongly dependent on the percentage of spotted area of the surface, while changes in spot distribution over the surface could result in changes of the amplitude of variability. FR Cnc has a short (for such class of objects) rotational period of 0.8267 d. As was shown in Dorren, Guinan & Dewarf (1994), this short rotational period leads us to expect large flare activity of the star.

The detection of a flare on FR Cnc on 2006 November 23 motivated us to continue photometric monitoring of this object as well as to study its archival *ASAS-3* observations (The All Sky Automated Survey; see Pojmanski (2002) for description of equipment and data pipeline).

2.1   ASAS Photometrical Observations

FR Cnc was observed in V-band with *ASAS-3* survey during 2002 December – 2008 May (6 observational seasons, see
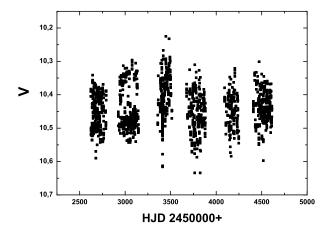
Figure 2. ASAS long term light curve

Fig. 2). All the data were split into separate data sets according to the 'seasonal gaps' in observations and folded with the 0.8267 d period (from Pandey et al. 2005) and represented in Fig. 3 (plotted twice for clarity). Table 1 represents the log of observations.

The initial epoch was common to calculate phases for all 6 phase diagrams and was chosen arbitrary as HJD (UTC) = 2452635.72669 (first point in dataset). No evidence of flares in the *ASAS-3* data was found. The vertical dashed line on Fig. 3 indicates the phase when the flare on 2006 November 23 occurred.

ASAS-3 data are not covering flare on 2006 November 23. Nearest *ASAS-3* observations were done on JD 2453881 and JD 24544091, what is 181 days before and 29 days after the flare. *ASAS-3* observations in 2006-2007 at a phase ∼0.88 (143 days after the flare) show that FR Cnc was brighter than during the rest of the time. This probably could be related to brightening episode, which was detected at the same phase during Terskol observations (see sect. 2.3).

Profiles of variability as well as the amplitude of variability are different from season to season, while the mean brightness remains constant ($V_{mean} = 10.439$ mag within the error limits of $\sigma = 0.017$ mag). To illustrate this, we plotted the amplitude and the mean brightness as a function of mean epoch of observations (Fig. 4). An abrupt decrease of amplitude in the year 2005 is clearly seen. One of the possible interpretations is continuous spottedness of the star and redistribution of spots/spot groups from season to season: i.e. spots didn't disappear, but distributed more uniformly over FR Cnc surface. To support this idea, notice the constancy of the mean brightness level. If spots disappear then increase of brightness and decrease of amplitude could be expected.

2.1.1 Periodogram Analysis

The data set was searched for periodic variation of brightness (in order to estimate with better accuracy the known rotational period) using the PERIOD04 package, developed by Patrick Lenz (Institute of Astronomy, University of Vienna, Austria; see Lenz & Breger 2005). Discrete Fourier transform (DFT) algorithm was applied for statistical analysis. Julian dates are heliocentrically corrected. The average zero point of 10.439 mag was subtracted to prevent the appear-

ance of additional features on the periodogram centered at frequency 0.0.

Making a periodicity analysis of *ASAS-3* photometry, we found a dominant frequency of $f = 1.209895$ c d^{-1}, while, as defined by equation 1, $\sigma(f) = 0.000022$ (therefore, period P = 0.826518 ± 0.000015 d; see Fig. 5). The detected periodicity could be interpreted as the rotational period and it is in good agreement with the period founded by Pandey et al. (2005), but with improved accuracy (due to the longer time span of *ASAS-3* observations). No other periodicity of FR Cnc brightness modulations was found on the basis of *ASAS-3* observations.

The DFT routine was applied separately to each season of observations as well. The obtained periodograms do not reveal any other significant periodicity, but only the same peak as for the periodogram for the whole time-string. The dominant frequency remains constant within the error limits of $\sigma(f) = 0.0003$ for all of 6 periodograms.

2.1.2 Estimation of Accuracy and Reliability of the Detected Period

Empirical results from observational analysis (Breger et al. 1993) and numerical simulations (Kuschnig et al. 1997) have shown that the ratio in amplitude in the periodogram between signal and noise should not be lower than 4.0 to give good confidence in the detected peak. We calculated the S/N-ratio from the periodogram for the determined dominant frequency, so S/N = 6.88.

The Spectral Window Function is important to confirm that the obtained frequencies are real or an artefact of the window function. This was done by assigning 1 to brightness values with the same observation times and checking the resulting diagram. There was no evidence of significant power at the location of the peak (Fig. 5). The dominant frequency on the spectral window is $F = 1.0027$ with amplitude $A = 0.9391$, which is due to daily gaps in observations.

Parameter uncertainties were calculated from an error matrix, which is a by-product of non-linear least-squares fitting procedure. Other types of uncertainties are those which could be calculated from analytically derived formulae assuming an ideal case. Based on some assumptions one can derive a formula for the uncertainties in frequency and signal amplitude at this frequency. See Montgomery & Odonoghue (1999) and Breger et al. (1999), Kallinger, Reegen & Weiss (2008) for the derivation based on a monoperiodic fit. The determined equation can be applied for each frequency separately:

$$\sigma(f) = \sqrt{\frac{6}{N}} \frac{1}{\pi T} \frac{\sigma(m)}{a} \qquad (1)$$

$$\sigma(a) = \sqrt{\frac{2}{N}} \sigma(m) \qquad (2)$$

where N is the number of time points, T is the time length of the data set, $\sigma(m)$ denotes the residuals from the fit and a refers to the signal amplitude at the particular frequency. Both 'analytical' and 'least-squares error matrix' calculations give similar results: $\sigma(f) = 0.000022$ and $\sigma(a) = 0.0037$. So, on the periodogram (Fig. 5) we plotted the $3\sigma(a)$-level (dashed line) to show that the detected peak exceeds it significantly.
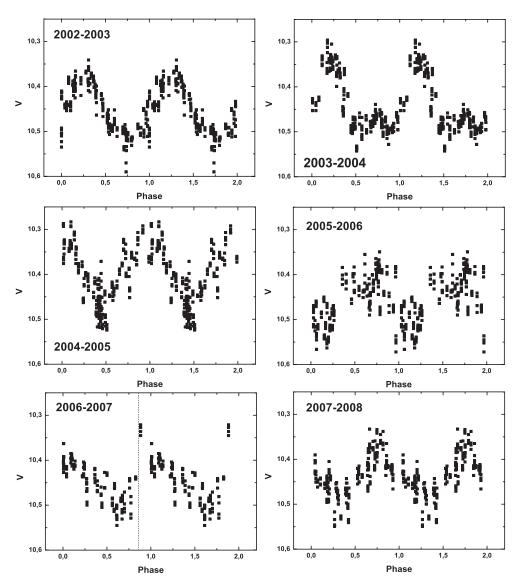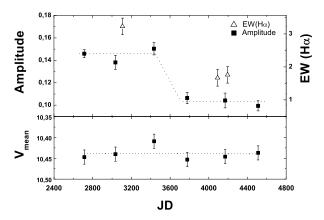
Figure 3. *ASAS-3* phase diagrams for six observing seasons. Please note that scales are the same for all plots. Vertical dashed line indicates the phase where the flare on 2006 November 23 was detected (see text for the explanation).

Another method for 1σ-level of amplitude calculation was proposed for use by R.A. Fisher (see Fisher 1935; Fisher 1936) and often called as Fisher Randomization Test. The idea is to take the original light curve and preserving the time column, shuffle the corresponding intensities around. That destroys any coherent signal in the light curve while keeping the time sampling intact. We are left with a shuffled light curve of pure white noise. The next step is to compute a DFT of this light curve which will look really noisy. The standard deviation of the average amplitude of such a DFT is close to the 1σ limit. We iterated this 25 times, therefore we use the average of 25 standard deviation values to determine 1σ-level. This pipeline gave us the value of $\sigma(a) = 0.0028$, which is slightly less than $\sigma(a)$ from 'analytical' and 'least-squares error matrix' calculations, hence we plotted the bigger value on our periodogram to be confident.

Figure 4. Mean amplitude of variability, *EW* of Hα and mean brightness of FR Cnc during the years 2002–2008. (See sect. 6.1 regarding Hα.)
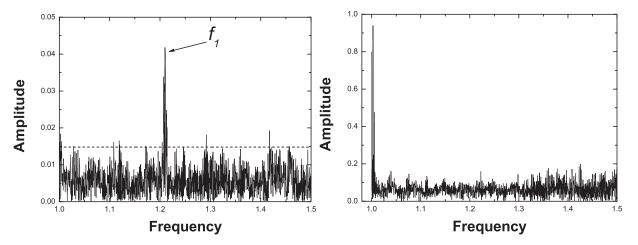
Figure 5. Periodogram of *ASAS-3* data in frequency range of 1.0–1.5 and Spectral Window

Table 1. Log of *ASAS-3*-observations of FR Cnc

Year	T_{start} 2450000+	T_{end} 2450000+	N_{points}
2002–2003	2635	2791	59
2003–2004	2924	3146	62
2004–2005	3357	3512	63
2005–2006	3674	3881	61
2006–2007	4091	4247	34
2007–2008	4409	4611	56

2.2   Photometric Sequence

We carried out the BVR_cI_c photometric calibration for 166 stars in the vicinity of FR Cnc with V-magnitudes in the range 9.85–18.06 mag that could serve as comparison stars. Calibration was done at the Sonoita Research Observatory (Arizona, USA) using a robotic 0.35-m telescope, equipped with an SBIG STL-1001XE CCD camera. A table with this photometrical sequence is available electronically only via the AAVSO ftp-server[1]. For user convenience, we have used the ALADIN Sky Atlas (Bonnarel et al. 2000) to align our calibration data on a DSS2/STScI POSSII image[2].

2.3   Terskol Observations

Optical B-band photometry was carried out from 2007 March to 2008 February at Terskol Branch of the Astronomy Institute (Russia) with 29-cm telescope and Apogee-47 Alta CCD camera. All observations were made in the B-band as the flare amplitude is expected to increase with decreasing wavelength. The duration of each observing run varies from 2 to 7 h. See Table 2 for log of observations. The calibration process of the obtained frames, comparison and check stars remains the same as described by Golovin et al. (2007).

The mean amplitude of FR Cnc brightness variations in the B-band during the observations in the year 2007 was 0.12 mag and 0.13 mag in the year 2008. There are no peculiar features in the light curve from the year 2008, while in the photometry obtained in the year 2007 two brightening

Table 2. Log of Terskol photometric observations of FR Cnc in the years 2007–2008

Year	Beginning of the Run (HJD)	End of the Run (HJD)
2007 March	2454171.2453	2454171.4361
	2454174.3501	2454174.4019
	2454180.1863	2454180.4691
	2454182.2395	2454182.4972
	2454188.4424	2454188.4721
2008 February	2454498.4150	2454498.5233
	2454500.2675	2454500.5345
	2454501.1575	2454501.5403
	2454502.1681	2454502.5870
	2454503.2157	2454503.4481
	2454504.1755	2454504.3025

episodes were detected: namely, on 2454180.3 and 2454182.3 (see Fig. 6). Amplitude in B-band was 0.06 and 0.12 mag respectively. It has to be noted that the second episode (HJD = 2454182.3) occurred at the same phase as the flare of 2006 November 23 (phase = 0.88). Probably both the events (flare on 2006 November 23 and brightening episode at phase 0.88) are originated from the same long-living active regions on the surface of FR Cnc.

3   POLARIMETRIC OBSERVATIONS

The BVR broad-band polarimetric observations of FR Cnc were obtained on 2007 October 19 and 20 using TK 1024 pixel^2 CCD camera mounted on the Cassegrain focus of the 104-cm Sampurnanand Telescope of ARIES, Nainital (India). The optical imaging polarimetry was carried out in B, V and R ($\lambda_{B_{\text{eff}}} = 0.440$ μm, $\lambda_{V_{\text{eff}}} = 0.550$ μm and $\lambda_{R_{\text{eff}}} = 0.660$ μm,) photometric bands.

Standard stars for null polarization and for the zero-point of the polarization position angle were taken from Schmidt et al. (1992). The results for standards are given in Table 3. From the results, it can be concluded that obtained values of polarization and position angles are in good agreement with Schmidt et al. (1992) within the error limit.

Both the program and the standard stars were observed during the same night. HD 25433 and HD 19820 (= CC Cas)
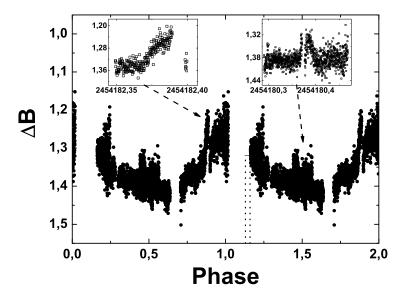
Figure 6. *B*-band Photometry at Terskol Observatory in 2007 March. Plotted twice for clarity. Dotted lines denote phases when polarimetric observations were done. Note an enlarged plots of brightening episodes on JD = 2454180 and JD = 2454182.

Table 3. Observed polarized standard stars.

Star name	Filter	$P\pm\epsilon_P(percent)$	$\theta\pm\epsilon_\theta(^\circ)$	$P\pm\epsilon_P(percent)$	$\theta\pm\epsilon_\theta(^\circ)$
		Published data		This paper	
HD 25433	B	5.23±0.09	134.3±0.05	5.17±0.21	135.6 ±1.0
	V	5.12±0.06	134.2±0.03	5.13±0.09	133.5 ±0.8
	R	4.73±0.05	133.6±0.03	4.76±0.13	132.9 ±0.5
HD 19820	B	4.70±0.04	115.70±0.22	4.66±0.07	115.49 ±0.19
	V	4.79±0.03	114.93±0.17	4.76±0.10	114.15 ±0.20
	R	4.53±0.03	114.46±0.17	4.56±0.17	114.18 ±0.21

were used as a standard polarized stars, while HD 21447 and G 191-B2B (= HIP 23692) served as standard unpolarized stars.

The results are listed in Tables 3, 4 and 5, where P is the fraction of the total light in the linearly polarized condition and θ is the position angle of polarization plane to the equatorial plane. It is denoted by the normalized Stokes' parameter q (= Q/I), when the half wave plate's fast axis is aligned to the reference axis ($\alpha = 0^\circ$). Similarly, the normalized Stokes' parameter u (= U/I), when the half wave plate is at 22.5°. For further details on used equipment and the method of observations, refer to Medhi et al. (2007).

By dotted lines on the lightcurve we indicate the phases ($\varphi_1 = 0.16, \varphi_2 = 0.13$ for 2007 October 19 and 20 respectively), when our polarimetric observations were conducted (see Fig. 6). FR Cnc was in maximal brightness during that time.

Polarization in FR Cnc could be magnetic in origin. The degree of polarization depends nonlinearly on the size of magnetic regions (see Huovelin & Saar 1991; Saar & Huovelin 1993). These authors have also calculated a grid of expected degrees of polarization in $UBVRI$ band for stars with temperature from 4000 to 7000 K and log g from 2.0 to 4.5. We have used their results to compare our observed values of polarization for FR Cnc. Fig. 8 represents the degree of polarization for FR Cnc in BVR bands.

The maximum possible degree of polarization for the total spot area of 24 per cent is derived from the calculations of Saar & Huovelin (1993) for the star corresponding to the spectral type of K5–7V and characteristic magnetic field of 2.7 kG. These values are over-plotted and represented by a solid line in Fig. 8. The observed polarization in the B band is in good agreement with the theoretical values expected for Zeeman polarization model. However, the observed polarization in V and R bands slightly exceeds the theoretical values.

Model values for K2V-K7V and K2IV-K2V spectral types appear to be even lower and certainly do not match the polarization in any of observed bands. This is also observed in some other young spotted stars (MS Ser, LQ Hya, VY Ari; see Alekseev 2003) and probably due to the presence of a supplementary source of linear polarization.

The predicted values of polarization due to Thompson and Rayleigh scattering from inhomogeneous regions are not enough to explain the observed polarization excess (Thompson and Rayleigh scattering for the assumed spectral type supposed to be of order of 10^{-7} and 10^{-4} per cent respectively; Saar & Huovelin 1993). The mechanism which can produce additional linear polarization is probably scattering in circumstellar material (e.g. see Pandey et al. 2009); on the other hand, the mentioned models are unacceptable if
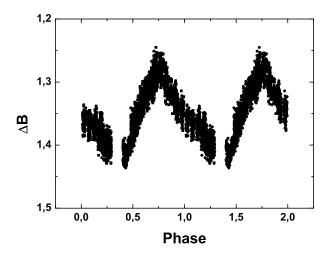
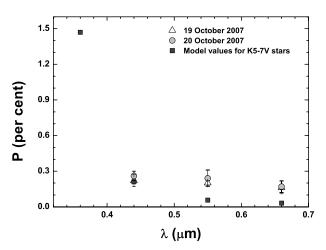**Figure 7.** *B*-band Photometry at Terskol Observatory in 2008 February.

Table 4. Observed unpolarized standard stars

Star name	Filter	q	u
HD 21447	B	0.019	0.011
	V	0.037	-0.031
	R	-0.035	-0.039
G191B2B	B	0.072	-0.059
	V	-0.022	-0.041
	R	-0.036	0.027

FR Cnc is a close binary star (Alekseev 2003; Elias & Dorren 1990 and Saar & Huovelin 1993).

4 SPECTROSCOPIC OBSERVATIONS

A total of 58 high and low resolution spectra of FR Cnc have been obtained and analysed in this work. The spectroscopic data were obtained during five observing runs. Details of each observing run are given in Table 6: date, telescope, spectrograph, CCD chip, spectral range covered, number of

Figure 8. The degree of polarization of FR Cnc as a function of wavelength. Model values of polarization for K5-7V spectral types stars (Saar & Huovelin, 1993) are plotted for comparison.

orders included in each echelle spectrum, range of reciprocal dispersion, spectral resolution (determined as the full width at half maximum, FWHM, of the arc comparison lines) and mean S/N in the Hα line region.

The spectra were extracted using the standard reduction procedures in the IRAF[3] echelle package (bias subtraction, flat-field division and optimal extraction of the spectra). We obtained the wavelength calibration by taking spectra of a Th-Ar lamp. Finally, we normalized the spectra by a polynomial fit to the observed continuum.

5 STELLAR PARAMETERS

Stellar parameters of FR Cnc are given in Table 7 and Table 8. The photometric data ($B - V$, V), P_{phot}, projected rotational velocity ($v \sin i$), and galactic space-velocity components (U, V, W) have been determined in this paper. The astrometric data (parallax, π; proper motions, $\mu_\alpha \cos \delta$ and μ_δ) are from *Hipparcos* and *Tycho-2* catalogues (ESA 1997).

5.1 Spectral classification

FR Cnc is classified as a K8V-star by Schachter et al. (1996), while a multicolour photometric study allowed Pandey et al. (2005) to classify it as a K5V-star. They also have obtained the Spectral Energy Distribution (SED) of the star matching a T_{eff} of 4250±250 K and a log g of 4.50±0.5, that agrees with a K5V classification.

We have compared our high resolution echelle spectra, in several spectral orders free of lines sensitive to chromospheric activity, with spectra of inactive reference stars of different spectral types and luminosity classes, observed during the same observing run. This analysis makes use of a modified version of the program STARMOD (JSTARMOD) developed at Penn State University (Barden 1985; López-Santiago et al. 2010). This program constructs a synthesized stellar spectrum from artificially rotationally broadened, radial-velocity shifted, and weighted spectra of appropriate reference stars. For FR Cnc, we have obtained the best fit with a K7V reference star, which is in closer agreement with the K8V classification rather with the K5V from Pandey et al. (2005).

5.2 Radial Velocity

We have determined the heliocentric radial velocities (RV hereafter) by making use of cross-correlation technique (see e.g. Gálvez et al. 2007). The spectra of the target were cross-correlated order by order, using the routine FXCOR in IRAF, against spectra of RV standards with similar spectral type taken from Beavers et al. (1979). We derived the RV for each order from the position of the peak of the cross-correlation function (CCF) and calculated the uncertainties based on the fitted peak height and the antisymmetric noise as described by Tonry & Davis (1979).

---

[3] IRAF is distributed by the National Optical Observatory, which is operated by the Association of Universities for Research in Astronomy, Inc., under contract with the National Science Foundation.

Table 5. Observed BVR polarization values for FR Cnc.

Date of Observation	Filter	Time (UT)	$P \pm \epsilon_P (percent)$	$\theta \pm \epsilon_\theta (°)$
October 19, 2007	B	22:22:12.0	0.22 ±0.05	57 ±7
	V	22:01:45.1	0.20 ±0.02	55 ±2
	R	22:10:52.6	0.16 ±0.05	61 ±7
October 20, 2007	B	21:25:36.6	0.26 ±0.04	55 ±5
	V	21:30:00.5	0.24 ±0.07	54 ±6
	R	21:35:48.6	0.17 ±0.05	58 ±7

Table 6. Description of spectroscopic observations

Number	Date (dd/mm/yyyy)	Telescope	Instrument	Detector	Spect. range (Å)	Orders	Dispersion (Å)	FWHM[1] (Å/pixel)	S/N Hα
1	29/03–07/04/2004	2.2-m[a]	FOCES[d]	2048x2048 24μ SITE#1d	3450–10700	112	0.04–0.13	0.08–0.035	40
2	11–13/04/2004	2.0-m[b]	HFOSC[e]	2000x4000 SiTe ST-002, grism Gr14	3270–6160	1	3.57	7.23–1.47	200
				2000x4000 SiTe ST-002, grims Gr8	5800–8350	1	3.23	3.66–3.99	200
3	16–21/12/2006	2.2-m[a]	FOCES[d]	2048x2048 24μ SITE#1d	3600–10700	106	0.08–0.1	0.08–0.04	40
4	24–26/02/2007 07–08/05/2007	2.2-m[a]	FOCES[d]	2048x2048 24μ SITE#1d	3600–10700	106	0.04–0.13	0.07–0.41	40
5	21/03/2008	NOT[c]	FIES[f]	2000x2000 EEV42-40	3620–7360	80	0.02–0.04	0.05–0.11	80

[1] Full Width at Half Maximum of the arc comparison lines;
[a] 2.2-m telescope at the German-Spanish Astronomical Observatory (CAHA, Almería, Spain);
[b] 2.0-m Himalayan Chandra Telescope at the Indian Astronomical Observatory (Mt. Saraswati, Hanle, India);
[c] Nordic Optical Telescope (NOT) at the Observatorio del Roque de los Muchachos (La Palma, Spain);
[d] The Fibre Optics Cassegrain Echelle Spectrograph (FOCES);
[e] Himalaya Faint Object Spectrograph and Camera (HFOSC);
[f] The high-resolution Fibre-fed Echelle Spectrograph (FIES).

As Fig. 9 (top) shows, the irregular profiles of the CCF (double peaks and asymmetries) can produce significant errors in RV measures. These features show regular variations: a double peak moving on time-scale of the rotational period can be seen. Photospheric activity features on the stellar surface that disturb the profile of the photospheric lines could induce variations in the peak of the CCF, but a stellar companion could also produce the double peak effect.

We checked if these RV variations could be due to a binary nature of FR Cnc. We found no evidence for the existence of a companion by measuring the RV of the peaks and by trying to fit the data to a coherent orbit.

We also carried out a line bisector analysis to enable us to ascertain whether the RV variations may be attributed to starspots.

The CCF was computed for regions which include the photospheric lines commonly used in the Doppler Imaging technique, while excluding chromospheric and telluric lines (Queloz et al. 2001). We computed the bisector and, to quantify the changes in the CCF bisector shape, also the bisector inverse slope (BIS). The BIS was defined as the difference of the average values of the top and bottom zones (we avoided wings and core of the CCF profile, due to errors of bisectors measurements, which are large in these zones). We studied the bisector variations only for FOCES04 run, as it was the more suitable data for the study. Three cases are reported in bibliography (see for example Queloz et al. (2001), Martínez Fiorenzano et al. (2005), Bonfils et al. (2007), etc.): a) anticorrelation, which indicates that the RV variations are due to stellar activity (by active regions at the stellar surface like spots or plages), b)

lack of correlation, which indicates the Doppler reflex motion around the center of mass due to other bodies orbiting the star, c) correlation, which, as pointed out by Martinez-Fiorenzano et al. (2005), indicates that the RV variations are due to light contamination from an unseen stellar companion.

As shown in Fig. 10, there is an anticorrelation between BIS and RV, with a Pearson correlation coefficient (r) of -0.6851. This result suggests that the RV variations of FR Cnc are due to stellar activity variations (e.g. spots on photosphere) and not due to a binary nature. When the spectrum of the standard star was broadened to the same rotational velocity of FR Cnc, the profiles of the CCF became smoother and could be fitted with a Gaussian profile, (see Fig. 9, bottom).

The irregular profiles of the CCF (double peaks and asymmetries) can produce significant errors in RV measurements (see Fig. 9). These irregularities may come from photospheric activity features on the stellar surface. They can distort the profile of the photospheric lines and induce variations in the peak of the CCF. However, this behavior may be caused by the difference in rotational velocity ($v \sin i$) between the target and standard star (see e.g. Gálvez et al. 2007) when the standard is a much slower rotator than the target. The CCF is essentially the broadening function that would be applied to the template spectrum. Use of a broadened template removes higher moments introduced from the starspots, enabling a relatively unbiased estimate of RV to be determined (Fig. 9). A mean RV of 17.8 ± 1.6 is obtained for the 2004 data set and is in good agreement with the RV derived through optimisation of parameters in the

Table 7. Stellar parameters of FR Cnc

T_{sp}	V_{mean}	$B - V_{mean}$	P_{phot} (d)	$v \sin i$ (km s^{-1})	i $^{\circ}$
K7V	10.44	1.10	0.826518±0.000015	46.2±0.8	55

Table 8. Astrometric and kinematic parameters of FR Cnc

π (marcsec)	$\mu_{\alpha} \cos \delta$ (marcsec yr^{-1})	μ_{δ} (marcsec yr^{-1})	$U \pm \sigma_U$ (km s^{-1})	$V \pm \sigma_V$ (km s^{-1})	$W \pm \sigma_W$ (km s^{-1})	V_{Total} (km s^{-1})
30.24±2.03‡	-98.1±1.6‡	-91.0±1.5‡	-19.02±0.62	-18.99±1.08	-8.03±1.58	28.05

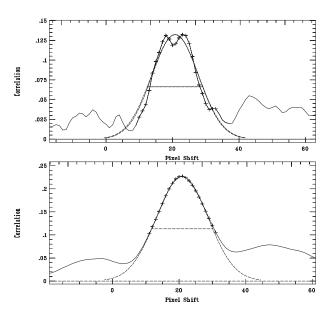‡ From *Hipparcos* and *Tycho* − 2 catalogues (ESA 1997).

Figure 9. (Top) An example of CCF of FR Cnc in FOCES04 observing run. Irregular profiles can be seen in the peak. These irregularities can produce significant errors in RV determination. (Bottom) The same CCF obtained when we broadened the standard star to FR Cnc rotational velocity. Irregular profiles become smoother and could be fitted with a Gaussian.

Doppler imaging process (Section 7), where we find $V_{hel} = 18.6 \pm 0.6$. Therefore all the radial velocities given in this paper have been calculated by cross-correlation with this rotational broadened spectrum of the standard star.

In Table 9 we list, for each spectrum, the heliocentric radial velocities (V_{hel}) with their corresponding errors (σ_V) obtained as weighted means of individual values deduced for each order in the spectra. We also list data points from Upgren et al. (2002) for comparison.

Those orders which contain chromospheric features and prominent telluric lines have been excluded when determining the mean radial velocity.

5.3   Rotational Velocity

By using the program JSTARMOD (see Sect. 5.1) we have obtained the best fits for each observing run using $v \sin i$ values
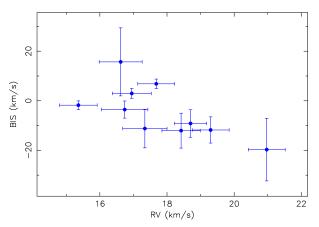

Figure 10. Bisector velocity span vs. RV for FOCES04 observing run. The clear negative correlation indicates that RV variations are due to stellar activity (see Sect. 5.2).

of $\approx$35 km s^{-1}. However, this value depends on the rotation of the standard star which has non-zero rotation. Therefore the obtained value can only be used as an approximation.

To determine an accurate rotational velocity of this star we made use of the following method (see Martínez-Arnáiz et al. 2010 for details). Rotational velocities, $v \sin i$ can be written as follows (see Queloz et al. (1998) and references therein):

$$\sigma_{rot}^2 = \sigma_{obs}^2 - \sigma_0^2 \Longrightarrow v \sin i = A \sqrt{\sigma_{obs}^2 - \sigma_0^2} \qquad (3)$$

where A is a coupling constant which depends on the spectrograph and its configuration. The spectrum of each of these stars was broadened using the program JSTARMOD from $v \sin i = 1$ km s^{-1} up to 50 km s^{-1} and the respective CCF was calculated. A was found for every spectrograph by fitting the relation $(v \sin i)^2$ vs σ_{obs}^2. It is well known that σ_0 is a function of the broadening mechanisms which are present in the atmosphere of the star, except rotation (Melo et al. 2004). Since the broadening mechanisms are function of the temperature and gravity, we may expect a dependence of σ_0 on the temperature. To determine this dependence we use synthetic spectra with no rotational velocity computed using the ATLAS9 code by (Kurucz 1993) adapted to work under a Linux platform by Sbordone et al. (2004) and Sbordone (2005). Once A is determined and σ_0

Table 9. Radial and Rotational Velocities

Run	HJD (2400000 +)	$V_{hel} \pm \sigma_V$ (km s^{-1})	$\overline{vsini}$ (km s^{-1})
FOCES04	53098.3713	16.95 ± 0.58	44.1 ± 1.9
FOCES04	53099.3411	18.42 ± 0.57	
FOCES04	53099.4230	17.34 ± 0.66	
FOCES04	53099.4546	16.74 ± 0.69	
FOCES04	53100.3156	16.62 ± 0.64	
FOCES04	53100.3917	15.36 ± 0.56	
FOCES04	53101.3264	18.70 ± 0.48	
FOCES04	53101.4495	20.97 ± 0.55	
FOCES04	53102.3306	19.30 ± 0.55	
FOCES04	53102.4753	17.68 ± 0.55	
FOCES06	54086.6770	19.85 ± 0.63	37.2 ± -
FOCES06	54088.5918	19.62 ± 0.45	
FOCES06	54091.6192	20.45 ± 0.53	
FOCES07a	54156.4482	19.98 ± 0.52	41.3 ± 2.7
FOCES07a	54158.5625	20.41 ± 0.80	
FOCES07b	54228.3461	-	43.6 ± 3.2
FOCES07b	54229.3496	-	
FIES08	54547.4408	17.82 ± 0.74	-
Upgren02	51626.695	27 ± 2.3	-
Upgren02	51626.730	24 ± 4.1	-

calibrated with the color index $(B - V)$, σ_{obs} (width of the CCF of the star when is correlated with itself) is measured for each star, $v\sin i$ can be directly calculated using the above formula (3).

In Table 9 we list, for each observing run, the averaged $v \sin i$ value obtained. From Table 9 we estimate uncertainties of 1.9-3.2 km s^{-1} based on the standard deviations as each measurement epoch. It is likely that the $v \sin i$ values vary by more than these uncertainties since FR Cnc is very active and exhibits starspots (see Section 7) that significantly distort the rotationally broadened absorption lines. Moreover, while the observations taken in the year 2004 cover a complete rotation cycle, those $v \sin i$ measurements at other epochs, only include one to two observations and are likely to yield more biased results (i.e. depending on the location of starspots at the observation phases). In Section 7, we model the line profile using our Doppler imaging code, allowing for the presence of spots. The resulting fits are thus likely to give a more accurate rotation velocity, $v \sin i$, for FR Cnc.

5.4 Kinematics

We computed the galactic space-velocity components (U, V, W) and their associated errors of FR Cnc using the procedure described by Johnson & Soderblom (1987) modified by López-Santiago (see Montes et al. 2001). This procedure uses J2000 coordinates and takes into account correlation in the measures of *Hipparcos*. We use averaged RV calculated here (18.63 ± 0.14 km s^{-1}) and the proper motions and parallax from *Hipparcos*.

The obtained values of the components with its module V_{Total} and associated errors are given in Table 8. The velocity components in the (U, V) diagram are clearly within the young disc population boundaries (Eggen 1984a,b, 1989; Montes et al. 2001a,b) indicating that the star belongs to the young disc and that it might also belong to the IC 2391 moving group, mentioned previously by Pandey et al. (2005),

but the Eggen kinematic criteria (see Montes et al. (2001) for details) are negative, showing that FR Cnc could be not a member of any moving group (MG hereafter) in the young disc area.

The classical view of MGs (e.g. Eggen 1984a), i.e. they come from the remnant of a star-forming cloud has been discussed in recent years. Several studies (e.g. Famaey et al. 2007, 2008; Antoja et al. 2008; Zhao et al. 2009) seem to support a dynamic or resonant mechanism origin. While both theories are feasible, we will just take into account that the percentage of contamination of the young disc space velocity area by old field population is high (see López-Santiago et al. 2009 and reference therein) and so age constraints are needed to assess if FR Cnc belongs to any of young disc moving groups.

5.5 The Li I λ6707.8 line

Li I λ6707.8 spectroscopic feature is an important diagnostic tool for assessing the age in late-type stars, since Lithium is destroyed easily by thermonuclear reactions in the stellar interior.

The spectral region of the resonance doublet of Li I at λ6708 Å is covered in all the high resolution observations. We measured the equivalent width (EW hereafter) in seven spectra.

Due to the small value, we were not able to measure EWs directly, or use spectral subtraction technique. Therefore EWs have been obtained using the IRAF task SBANDS, performing an integration within a band of 1.6 Å centred in the lithium line (Maldonado et al. 2010). We have obtained an averaged value of 54 mÅ. In our high resolution spectra the Li I line is blended with Fe I 6707.4 Å. To subtract the Fe I contribution we used the color-index relation from Favata (1993). Therefore, we obtain the final value of EW(Li I) to be 34 mÅ. In Fig. 11 we plot as an example, a spectra formed by co-adding the FOCES04 run spectra and we indicated the position of the Li I line.

By comparing this value with stars of similar spectral type (K5-K7 with V-I = 1.3) in other MGs members or clusters of a well-known age (in the same way as in Figure 3 of López-Santiago et al. 2009), it is in agreement with being a young object between 10-120 and compatible with being IC 2391 MG member.

5.6 Other age indicators

Ideally, further constraints on FR Cnc's age should be calculated to confirm its youth. Popular age approximations are for example the X-ray flux-age relation (Mamajek & Hillenbrand 2008; equation A3) or the commonly used relation between age and R'_{HK} index, that measures chromospheric emission in the cores of the broad chromospheric Ca II H & K lines (see e.g. Noyes et al. 1984; Baliunas et al. 1996; Mamajek & Hillenbrand 2008). The former relation is valid for stars with spectral types earlier than that of FR Cnc and so can not be used. Also, using the latter relation, from our Ca II H & K fluxes (see Sect. 6.3 and Table 9) we obtain a $\log R'_{HK}$ = -3.48 which is outside the validity range of the activity-age relation but in this case it is compatible with the young age.
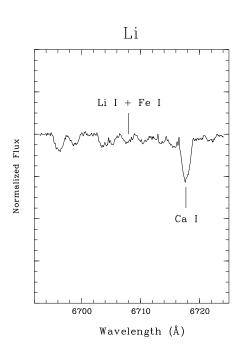
Figure 11. Spectrum in the Li I line region, resulting of co-adding the 10 observed spectra of FOCES04 run in order to increase the S/N. The position of the Li I + Fe I and Ca I are marked.
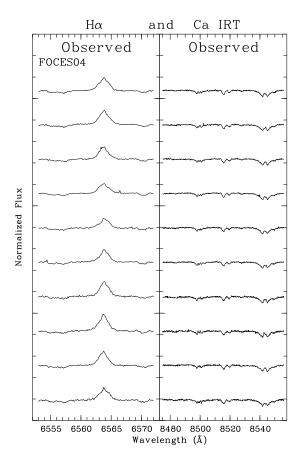

Figure 12. Spectra in the Hα (left side) and Ca II IRT $\lambda\lambda 8498$, 8542 (right side) line regions for FOCES04 observing run; clear wide and prominent emission arises over the continuum from Hα and a clear emission in the core of the absorption line is seen in the Ca II IRT lines.
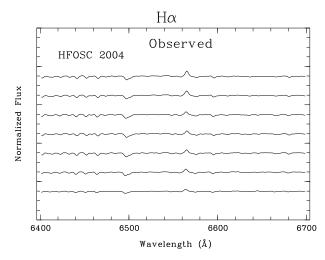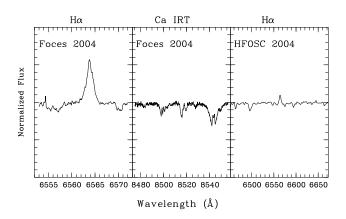
6 CHROMOSPHERIC ACTIVITY INDICATORS

Both echelle and long slit spectra analysed in this work allowed us to study the behavior of the different indicators from the Ca II H & K to the Ca II IRT lines, which are formed at different atmospheric altitudes. The chromospheric contribution to these features was determined by using the spectral subtraction technique described in detail by Montes et al. (2000) and Gálvez et al. (2002).

The excess emission EW of different spectral features were measured in the subtracted spectra. In Table 10 we give the EW for the Ca II H & K, Hϵ, Hδ, Hγ, Hβ, Hα, and Ca II IRT ($\lambda\lambda 8498$, 8542, 8662 Å) lines for the echelle spectra. These EWs were converted to an absolute surface fluxes by using the empirical stellar flux scales calibrated by Hall (1996) as a function of the star color index. In our case, we used the $B - V$ index and the corresponding coefficients for Ca II H & K, Hα and Ca II IRT, using for Hϵ the same coefficients as for Ca II H & K, and derived the Hδ, Hγ and Hβ coefficients of flux by carrying out an interpolation between the values of Ca II H & K and Hα. The logarithm of the obtained absolute flux at the stellar surface ($\log F_{\rm S}$) in ergs cm^{-2} s^{-1} Å^{-1} for the different chromospheric activity indicators is given in Table 11.

Fig. 12 shows representative observations in the Hα, and Ca II IRT $\lambda\lambda 8498$, 8542 line regions for high resolution spectra. Fig. 13 shows representative observations in the Hα for low resolution spectra. Fig. 14 shows a closer view of one spectrum from Figs. 12 and 13 where the emission can be better seen.
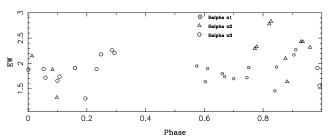

Figure 13. Sample of spectra in the Hα line region for HFOSC04 observing run; clear emission arises over the continuum from Hα in this low resolution spectra.

Figure 14. A representative spectra of Figs. 12 and 13, showing a zoom of the Hα (left side) and Ca II IRT (center) line regions for FOCES04 and Hα (right) line region for HFOSC04.

Figure 15. Variation of Hα *EW* vs phase in HFOSC04 run. Different symbols represent different nights. The second night is in triangles, showing higher values of the Hα *EW*s.
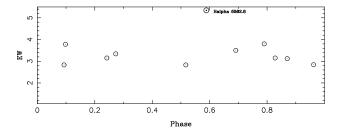
6.1 The Hα line

We analysed the Hα line region for all the spectra. This line in the obtained spectra is always observed in emission above the continuum (see Figs. 12 and 13).

Measuring the *EW* of this line, we found that the *EW* average of the Hα emission is quite different in every season, showing significant variability in time-scales of a year. $EW(\text{H}\alpha) = 3.23$ Å for FOCES04 run while, $EW(\text{H}\alpha) = 1.67$, 1.72 and 1.87 Å for FOCES06, FOCES07a and FOCES07b respectively, $EW(\text{H}\alpha) = 1.72$ for the only value of FIES08 run. For the low resolution spectra we have an average value (in 37 spectra taken during three consecutive nights) of $EW(\text{H}\alpha) = 2.14$ Å in HFOSC04 run.

Fig. 15 shows the variation of *EW* vs phase (calculated with the photometric period) in HFOSC04 run. Different symbols represent different nights. The second night (triangles) shows higher values of the Hα *EW*s. Top of Fig. 16, represent the variation of *EW* vs phase in the FOCES04 run.

Comparing the variations of Hα *EW* between the runs and the variation in each run when possible, we note activity level variations on a month-long timescale, from one year to the next (see Table 10). Making the comparison with the photometry, we notice a correspondence between marked variations in the light curve and $EW(\text{H}\alpha)$. In the year 2004 both photometry and spectroscopy show a high level of FR Cnc activity, while it is decreasing rapidly in the year 2005 and then remains on that level during our further
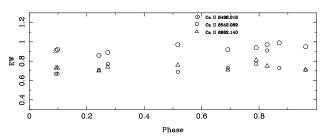

Figure 16. Top: Variation of Hα *EW* vs phase in FOCES04 run. Bottom: Variation of Ca II IRT *EW* vs phase.

observations. This can be interpreted as an activity cycle of at least 4–5 years, similar to Sun or other stars activity cycles, but further follow up is needed to confirm this. Accurate stellar activity cycle can prove useful for study the dynamo interface and activity cycle-rotation-spectral type mechanisms in the stars (see e.g. Lorente & Montesinos 2005).

The persistence of Hα emission indicates that it is a very active BY Dra system, but the vast range of variability levels make this star unusual and interesting for further study.

6.2 The Hβ, Hγ and Hδ lines

We can see the absorption of Hβ, Hγ and Hδ Balmer lines filled in with emission in the observed spectra. Fig. 17 plots a representative subtracted spectra of these three lines in different nights of FOCES04 run.

The variation of these lines with rotational phase and from season to season follows the same trend as Hα variation.

We also measured the ratio of excess emission in the Hα and Hβ lines ($\frac{EW(\text{H}\alpha)}{EW(\text{H}\beta)}$) and the ratio of excess emission $\frac{E_{\text{H}\alpha}}{E_{\text{H}\beta}}$ with the correction:

$$\frac{E_{\text{H}\alpha}}{E_{\text{H}\beta}} = \frac{EW(\text{H}\alpha)}{EW(\text{H}\beta)} \cdot 0.2444 \cdot 2.512^{(B-R)} \qquad (4)$$

given by Hall & Ramsey (1992). This corrects the absolute flux density in these lines for the color difference in the components. We have obtained a mean value of $\frac{E_{\text{H}\alpha}}{E_{\text{H}\beta}} \approx 2.5$. This value is in the limit between the presence of prominence-like material on or above the stellar surface (Buzasi 1989 and Hall & Ramsey 1992).

6.3 Ca II H & K and Hε

The Ca II H & K line region is included in most of the spectra but the efficiency of the spectrograph and the CCD decreases very rapidly due to the position of these lines at the end of
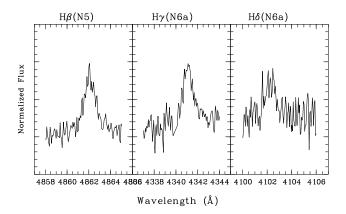
Figure 17. Representative subtracted spectra of Hβ, Hγ and Hδ lines in different nights of FOCES04 run.

the echellogram. Therefore, the obtained S/N ratio is very low, and the normalization of the spectra is very difficult. In many cases we could not measure the EW lines and in other we measured them in the observed spectra as it was not possible to apply the spectral subtraction for this region (see Tables 10 and 11).

Strong emission in the Ca II H & K is seen despite the low S/N.

6.4   Ca II IRT lines (λλ8498, 8542, and 8662)

The three lines of the Ca II (IRT) are included in all our echelle spectra. In all of them a clear emission arising in the core of the absorption lines is seen (see Fig. 12).

Averaged values of emission EW are $EW(\text{Ca II}) =$ 0.74, 0.93 and 0.81 Å for λλ8498, 8542, and 8662 in FOCES04 run. $EW(\text{Ca II}) = 0.49$, 0.72 and 0.61 Å in FOCES06 run. $EW(\text{Ca II}) = 0.66$, 0.86 and 0.70 Å in FOCES07a. $EW(\text{Ca II}) = 0.79$, 1.03 and 0.77 Å in FOCES07b and $EW(\text{Ca II}) = 0.71$, 0.89 and 0.79 Å in FIES08.

The variation of the emission in these lines is significant although not as strong as in Hα (see Table 10).

Only for the FOCES04-run we have enough data points to compare variations between Hα EWs and Ca II EWs. In other active stars a clear anticorrelation is usually seen (as their emissions come from different features in the stellar surface), see e.g. stars in Arévalo & Lázaro (1999), Montes et al. (2000), Gálvez et al. (2002), Gálvez et al. (2009) etc., but it is very weak in the case of FR Cnc (see Fig. 16).

In addition, we have calculated the ratio of excess emission EW, $\frac{E_{8542}}{E_{8498}}$, which is also an indicator of the type of chromospheric structure, which produces the observed emission. In solar plage values of $\frac{E_{8542}}{E_{8498}} \approx 1.5$–3 are measured, while in solar prominence the values are ≈ 9, the limit of an optically thin emitting plasma (Chester 1991). We have found a $\frac{E_{8542}}{E_{8498}} \approx 1.3$, indicating that Ca II IRT emission comes from plage-like regions.

7   DOPPLER IMAGING

Since FR Cnc is a rapid rotator with considerable broadening of spectral lines, we generated an indirect starspot map using the Doppler Tomography of Stars (DoTS) imaging code (Cameron 2001). In order to detect the line distortion due to starspots in the high resolution spectra, we have applied least-squares deconvolution (Donati et al. 1997; Barnes et al. 1998) to the 4362–6845 Å wavelength region of FOCES04 spectra (obtained at 2004 March – April). A single line, free of the effects of rotational line blending and with high S/N is thus derived. Deconvolution is carried out using a $T = 2450$ K model line list (VALD; see Kupka et al. 1999 & 2000) which indicates that there are 8345 lines in the selected wavelength region with normalized depths of 0.05–1.0. Regions around hydrogen Balmer lines, the Mg triplet and Na doublet are excluded from the deconvolution. A single line profile with a mean of $\lambda = 5460.4$ Å is derived for each observed spectrum. The mean S/N of the input spectra over the entire 4362Å - 6845Å wavelength region was 21.8, while the mean deconvolved line profiles possess S/N = 1008 (indicating a gain of 46.2). It should be noted that while the profile shown in Fig. 9 (upper panel) represents the broadening function of FR Cnc (i.e. rotational velocity plus starspot distortions), the LSD profiles in Section 7 are deconvolved using a linelist rather than a template. As such, the LSD profiles still contain the intrinsic stellar profile, and any distortions due to starspots will appear to possess a lower amplitude when compared with a template-derived CCF.

For the imaging procedure, we used the standard star, HD 151877, to represent the local intensity profile of a slowly rotating star. A two temperature model with $T_{\text{phot}} = 4250$ K and $T_{\text{spot}} = 3000$ K was used. The starspot image therefore represents the spot filling factor. Details of the Doppler imaging technique can be found in Cameron (2001). We optimized the goodness of fit to the 10 deconvolved profiles for heliocentric RV, axial inclination, equivalent width and $v \sin i$, finding $V_{hel} = 18.6 \pm 0.6$, $v \sin i = 46.2 \pm 0.8$ km s^{-1} and i $= 55 \pm 5°$. The $v \sin i$ value is higher than, but still consistent with, our mean $v \sin i$ value derived in Section 5.3. Since we here use all rotation phases to derive our best fit Doppler image, it is likely that the result is less biased than the previous results in Section 5.3 that do not take account of the presence of starspots, which affect the profile shape. Starspot distortions in the wings of the profiles for instance, are likely to lead to underestimations of $v \sin i$ when using a single spectrum, leading to a systematically lower mean estimation of $v \sin i$. We note however that our result for the 2004 observations is consistent with the value tabulated in Table 9 (i.e. 44.1 ± 1.9 km s^{-1}). Fig. 18 shows the deconvolved profiles (and phases of observation) while Fig. 19 shows mercator projections of the starspot image of FR Cnc.

The surface map in Fig. 19 (upper panel) indicates that FR Cnc possesses considerable spot coverage as suggested by the time varying distortions in the deconvolved profiles in Fig. 18 (left panel - spectroscopic data only). For comparison with the 2003 - 2004 (JD = 2452934-2453146 in Table 1) lightcurve presented in Fig. 3 (top right), we have generated a synthetic lightcurve based on the spectroscopically derived image in Fig. 19 (upper panel). While we are able

to recover the observed lightcurve morphology, we considerably *underestimate* the amplitude (Fig. 20, upper panel). This is likely due, at least in part, to loss of information in the Doppler imaging process (i.e. of the spectroscopic data) owing to resolution and noise constraints imposed by the fitting procedure which must optimise both the fit and the image entropy. With higher S/N ratio data and spectral resolution it is probable that more precise fitting would yield spot filling factors indicating cooler spots. In addition, there is a tendency for spots close to the equator ($<20°$) to be reconstructed at slightly higher latitudes than they are physically situated. This is due to the smaller entropy penalty of placing a smaller spot away from the equator as compared with a larger spot nearer the equator. The resulting spot distribution will naturally lead to predicted lightcurves with underestimated amplitudes since equatorial spots yield higher amplitudes.

We find a spot filling factor of 6 per cent from our spectroscopic Doppler image. This is at the lower end of the typical values (up to ~ 30 per cent) found for active stars by O'Neal, Saar & Neff (1996), O'Neal, Neff & Saar (1998) and O'Neal et al. (2004) using TiO indicators. We have therefore reconstructed an image that also makes use of the 2003/2004 V-band photometric data (e.g. see Barnes et al. 1998). It should be noted that while the lightcurve data spans several months, the spectroscopic data were taken over only a few days. Since the photometric observations taken within $\pm$ 1 month of the spectroscopic data do not show significant deviation from the photometric dataset as a whole, we made use of all photometric points. The resulting simultaneous fits to the data are shown in Fig. 18 (right panel) and Fig. 20 (bottom panel), while the reconstructed image is shown in Fig. 19 (bottom panel). Simultaneous imaging that makes use of spectroscopic and photometric data must strike a balance, such that reasonable fits to both data sets are achieved. We have already outlined (above) possible modest biases in an image derived from a spectroscopic fit to finite S/N. Lightcurve data alone does not contain sufficient information to make reliable images of single stars. Any complex spot structure or spot groups will be rendered simply as a single spot. Photometric imaging favours reconstruction at lower latitudes because a smaller spot is more easily able to reproduce the amplitude variation (and yields a lower image entropy penalty) in an observed lightcurve than a slightly larger spot at higher latitude. Allowing the photometric fit to more closely match the observed lightcurve results in a slightly poorer fit to the spectroscopic data. The fitted lightcurve now closely matches the observed lightcurve, since more large scale (albeit unresolved) starspot structure has been recovered. This has necessitated some loss of image details (Fig. 19, lower panel) as compared to the spectroscopic reconstruction alone (Fig. 19, upper panel). The filling factor is now greater at 9 per cent, adding further weight to the argument that spectroscopy alone is unable to recover all starspot information. Indeed, if the results from TiO are to be believed, there may be further unresolved global starspot coverage on FR Cnc and all other stars that have been subjected to such studies.

We also carried out a bisector analysis on the LSD profiles, calculating the bisectors in the same way as in Sect. 5.2. As we have mentioned, the LSD profiles should show a smoothing of the bisectors, reflected in the lower value of
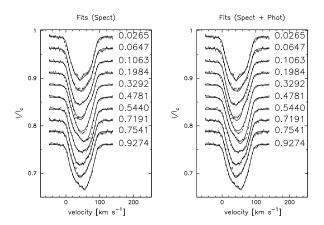

Figure 18. The figure shows the deconvolved profiles, with the phases of observation. The variation of the profile shape, due to starspots rotating into and out of view, is clearly seen.

the bisector we obtained comparing with the original spectra. As expected, the anticorrelation is still seen, but here we have a strongest Pearson correlation coefficient of r = -0.8992.

As might be expected for such an active star, FR Cnc exhibits a high degree of spot coverage. No spots are visible in the phase range $0.1 - 0.3$. This agrees well with the photometric V-band light curve plotted for the same period (Fig. 3, 2003–2004) which shows a maximum at phase ~ 0.2. This contrast with a significant degree of spotness at other longitudes is likely responsible for the high degree of photometrical modulation seen in this star. The starspot distribution of FR Cnc is also of interest since it is one of the latest spectral types to have been imaged. Comparison with the K5V rapid rotator LO Peg, Barnes et al. (2005), shows a significantly different spot distribution. While LO Peg rotates more rapidly ($v \sin i = 65.9$ km s^{-1}), showing predominantly mid-high latitude spot structures and a polar spot, FR Cnc shows only mid-latitude starspots. Small scale spot structure is expected to be variable on a day-long timescale, while Jeffers et al. (2007) have shown that the polar spot on the K0V star, AB Dor, is variable in extent over periods of years. While G, and K stars such as AB Dor often show strong polar caps, no such features were seen on the M1–M2 dwarf stars HK Aqr and RE 1816+541 (Barnes et al. 2001). This change in starspot location (i.e. with latitude) may be due to a change from a convective shell-type dynamo to a fully convective dynamo. Predominantly mid-high latitude spots are expected to arise from a rapidly rotating solar-like dynamo (Schüssler et al. 1996; Granzer et al. 2000) while a distributed dynamo may be expected to produce spots at all latitudes. However, only further spectroscopic time series observations of FR Cnc, with a higher cadence of observations (enabling better surface resolution to be obtained), would reveal the long term stability of the starspot patterns.

8   SUMMARY AND CONCLUSIONS

We have carried out a photometric, polarimetric and spectroscopic study of FR Cnc.

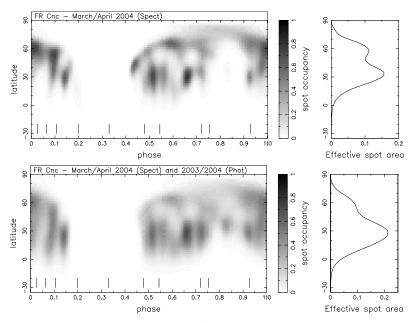Optical B-band photometry was carried out during

Figure 19. Mercator projection of the starspot image of FR Cnc. A high degree of spot coverage is revealed. There are no visible spots in the phase range 0.1 − 0.3. FR Cnc shows only mid-latitude starspots and no polar spot like other typical late K stars. The vertical lines mark the corresponding phase for 10 spectra we have used for deconvolution. The right hand plot shows how the mean effective spot area changes with latitude.

Table 10. *EW* of Chromospheric Indicators

Run	HJD (2400000+)	CaII								CaII IRT		
		K	H	$H\epsilon$	$H\delta$	$H\gamma$	$H\beta$	$H\alpha$	$\lambda 8498$	$\lambda 8542$	$\lambda 8662$
FOCES04	53098.3713	‡	‡	‡	‡	0.42	1.13	2.83	0.69	0.97	0.76
FOCES04	53099.3411	2.46	‡	‡	0.62	1.10	1.32	3.50	0.73	0.92	0.71
FOCES04	53099.4230	‡	‡	‡	‡	0.40	1.44	3.80	0.77	0.94	0.81
FOCES04	53099.4546	‡	‡	‡	‡	0.46	1.10	3.15	0.91	0.97	0.75
FOCES04	53100.3156	1.54	2.74	1.70	0.21	0.67	1.30	3.12	0.73	0.99	2.18
FOCES04	53100.3917	1.58†	1.47	0.73	0.25	0.30	1.03	2.84	0.71	0.95	0.71
FOCES04	53101.3264	‡	‡	‡	0.40	0.76	1.08	2.83	0.67	0.91	0.73
FOCES04	53101.4495	‡	‡	‡	‡	0.27	1.23	3.15	0.71	0.86	0.70
FOCES04	53102.3306	2.12	1.74	1.02	‡	0.77	1.21	3.78	0.67	0.92	0.73
FOCES04	53102.4753	‡	‡	‡	‡	‡	1.40	3.34	0.77	0.89	0.74
FOCES06	54086.6770	6.58▲	6.82▲	0.00▲	0.36	0.30	0.74	1.49	0.29	0.63	0.58
FOCES06	54088.5918	3.72▲	4.30▲	1.00▲	0.26	0.73	0.50	1.93	0.59	0.53	0.66
FOCES06	54091.6192	5.84▲	5.39▲	0.90▲	0.37	0.36	0.58	1.60	0.60	0.99	0.58
FOCES07a	54156.4482	9.69▲	5.97▲	1.40▲	0.32	0.24	0.74	1.80	0.68	0.86	0.71
FOCES07a	54158.5625	9.58▲	3.78▲	0.48▲	-	0.13	0.76	1.65	0.64	0.86	0.69
FOCES07b	54228.3461	-	-	-	-	-	-	1.87	0.79	1.03	0.77
FOCES07b	54229.3496	-	-	-	-	-	-	1.72	0.71	0.89	0.79

† Values measured with low S/N.
‡ Values not measured due to the low S/N.
▲ Values measured in the observed spectra (spectral subtraction is not applied).

2007 March − 2008 February at Terskol Branch of the Astronomy Institute (Russia). There are no peculiar features in the 2008 light curve, while in the 2007 photometry two brightening episodes were detected. One of them occurred at the same phase as the flare of November 23, 2006 (phase = 0.88) and probably indicates that both of these events (i.e. the flare on November 23, 2006 and the photometric brightening episode) originated from the same long-living active region on FR Cnc. The non-detection of any other flares in our photometry except 2006 November 23 implies that FR Cnc has a low frequency of flares.

We analysed *ASAS-3* photometry obtained in 2002– 2008 in *V*-band. No evidence of flares in *ASAS-3* data were found. The profiles of variability are different from season to season. The mean magnitude in *V*-band remained the same ($V_{\mathrm{mean}} = 10.439$ mag) during 2002–2008, while the amplitude decreased abruptly in 2005. The proposed interpretation is a redistribution of spots/spot groups over the surface of the star, while the total percentage of the spotted area was assumed to be constant within the error limits. A detailed periodogram study of the *ASAS-3* photometric data enabled us to derive a more accurate value for the pe-

Table 11. Emission Fluxes

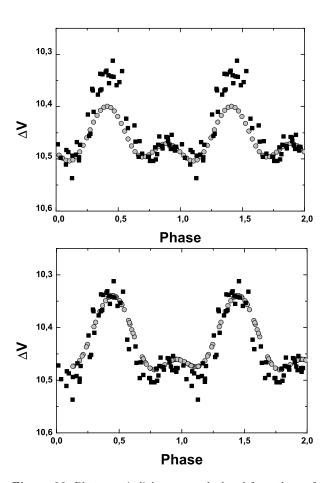| Run	HJD (2400000+)	CaII K	CaII H	Hε	Hδ	Hγ	Hβ	Hα	CaII IRT λ8498	CaII IRT λ8542	CaII IRT λ8662
FOCES04	53098.3713	‡	‡	‡	‡	5.88	6.35	6.91	6.24	6.38	6.28
FOCES04	53099.3411	6.62	‡	‡	6.03	6.30	6.42	7.00	6.26	6.36	6.25
FOCES04	53099.4230	‡	‡	‡	‡	5.86	6.46	7.04	6.28	6.37	6.31
FOCES04	53099.4546	‡	‡	‡	‡	5.92	6.34	6.95	6.36	6.38	6.27
FOCES04	53100.3156	6.41	6.66	6.46	5.56	6.08	6.41	6.95	6.26	6.39	6.74
FOCES04	53100.3917	6.42[†]	6.39	6.09	5.63	5.73	6.31	6.91	6.25	6.37	6.25
FOCES04	53101.3264	‡	‡	‡	5.84	6.14	6.33	6.91	6.22	6.36	6.26
FOCES04	53101.4495	‡	‡	‡	‡	5.69	6.39	6.95	6.25	6.33	6.24
FOCES04	53102.3306	6.55	6.47	6.23	‡	6.14	6.38	7.03	6.22	6.36	6.26
FOCES04	53102.4753	‡	‡	‡	‡	‡	6.45	6.98	6.28	6.35	6.27
FOCES06	54086.6770	6.74[▲]	6.75[▲]	–	5.49	5.45	5.92	6.46	5.76	6.09	6.06
FOCES06	54088.5918	6.49[▲]	6.55[▲]	5.92	5.36	5.84	5.75	6.57	6.06	6.02	6.11
FOCES06	54091.6192	6.68[▲]	6.65[▲]	5.87	5.50	5.53	5.81	6.49	6.07	6.29	6.05
FOCES07a	54156.4482	6.91[▲]	6.70[▲]	6.06	5.45	5.35	5.91	6.54	6.13	6.23	6.15
FOCES07a	54158.5625	6.90[▲]	6.50[▲]	5.60	–	5.10	5.93	6.50	6.10	6.22	6.13
FOCES07b	54228.3461	–	–	–	–	–	–	6.56	6.19	6.31	6.18
FOCES07b	54229.3496	–	–	–	–	–	–	6.52	6.14	6.24	6.19

Notes as in previous table.

Figure 20. Photometric lightcurves calculated from the surface maps and superimposed on *ASAS-3*-lightcurve for corresponding season of observations.

riod of FR Cnc. We find that $P = 0.08265 \pm 0.000015$ d. In addition, we also presented BVR_cI_c photometric calibration of 166 stars in FR Cnc vicinity, whose V-magnitude is in the range of 9.85–18.06 mag.

The BVR broad-band polarimetric observations of FR Cnc have been obtained at ARIES in Nainital (India) at Manora Peak. The observed polarization in B-band is well matched with the theoretical values expected for Zeeman polarization model. However, the observed polarization in V and R bands slightly exceeds the theoretical values and Thompson and Rayleigh scattering from inhomogeneous regions are not enough to explain the observed polarization excess. Therefore the excess of linear polarization should come from an additional source of polarization. Taking into account that we conclude that FR Cnc is not a binary, the mechanism which can produce additional linear polarization is probably scattering in circumstellar material distributed in an asymmetric geometry (e.g. see Pandey et al., 2009).

A total of 58 spectra of FR Cnc, which have been obtained in 2004–2008, were analysed in this work. Based on our spectroscopic observations, FR Cnc was classified as K7V star. RV analysis supports the single nature of FR Cnc. Anticorrelation between BIS and RV also indicates that the RV variations are due to stellar activity variations and not due to a secondary companion.

The kinematics study, based on obtained galactic space-velocity components (U, V, W) of FR Cnc, shows that this star clearly lies in the young disc population velocity space and might also belong to IC 2391 moving group, although the Eggen kinematic criteria shows that FR Cnc may not be a member of any MG in the young disc area. The Li I $\lambda6707.8$ averaged EW measured is 34 mÅ, giving the spectral type of FR Cnc, it is in agreement with being a young object between 10–120 Myr.

The Hα line was always observed above the continuum in all the obtained spectra. Measuring the EW of this line, we found that the Hα emission EW average in every season is quite different. In 2004, as with the photometry, spectroscopic indicators of chromospheric activity show a high level of activity which decreased in 2005. The Ca II (IRT) is included in our echelle spectra. From the ratio of excess emission EW we found that in FR Cnc, Ca II emission comes from plage-like regions. We noticed that FR Cnc can show

an activity cycle of 4-5 years, although further follow up will confirm this periodicity.

Since FR Cnc is a rapid rotator, we generated an indirect starspot map using the Doppler Tomography of Stars imaging code. From it we derive $v \sin i = 46.2 \pm 0.8$ km s^{-1} and $i = 55 \pm 5°$. FR Cnc belongs to one of the latest spectral types to have been imaged with the Doppler Tomography.

We independently estimated a rotational velocity of FR Cnc during our observations using Queloz method (Sect. 5.3) and by the D.I. fits (Sect. 7). Although they are differences in the results of the two methods, they are consistent. In Table 7 we have put as the rotational velocity of FR Cnc, the value obtained in the D.I. as it is likely more accurate.

Despite the short rotation period and its late spectral type, FR Cnc shows very few flare events. It shows high level of activity as it is a young star, but an unusually short variability due to the redistribution of activity features on the stellar surface. While this variability is reflected in the changes of the amplitude of brightness, the mean brightness permanently is nearly constant, indicating that the percentage of stellar surface covered by spots is also constant. The spots location is also unusual, not showing a polar spot like other F–K stars do but a distribution more resembling those seen in M1–M2 dwarfs. Although this may be indicative of a distributed dynamo, the mid-high latitude spot locations are more suggestive of an interface dynamo under the action of rapid rotation. We can only speculate as to whether FR Cnc is representative of a regime in which a convective-shell-type dynamo gives way to a fully convective dynamo. Polarimetric observations of the magnetic field by Donati et al. (2008) and Morin et al. (2008) for example suggest that this occurs at a later spectral type of M4, whereas other chromospheric indicators show no obvious changes until later M spectral types (e.g. Mohanty & Basri 2003). Further spectroscopy with a higher cadence would enable more detailed maps to be derived, with multiple epochs enabling the evolution of starspots to be investigated.

REFERENCES

Alekseev I. Y., 2003, ARep, 47, 430

Antoja T., Figueras F., Fernández D., Torra J., 2008, A&A, 490, 135

Arévalo M. J. & Lázaro C., 1999, AJ, 118, 1015

Baliunas S. L., Nesme-Ribes E., Sokoloff D., Soon W. H., 1996, ApJ, 460, 848

Barden S. C., 1985, ApJ, 295, 162

Barnes J. R., Collier Cameron A., Unruh Y. C., Donati J. F., Hussain G. A. J., 1998, MNRAS, 299, 904

Barnes J. R., Collier Cameron A., 2001, MNRAS, 326, 950

Barnes J. R., Cameron A. C., Lister T. A., Pointer G. R., Still M. D., 2005, MNRAS, 356, 1501

Beavers W. I., Eitter J. J., Ketelsen D. A., Oesper D. A., 1979, PASP, 91, 698

Bessell M. S., 1979, PASP, 91, 589

Bonfils X. et al., 2007, A&A, 474, 293

Bonnarel F. et al., 2000, A&AS, 143, 33

Breger M. et al., 1993, A&A, 271, 482

Breger M. et al., 1999, A&A, 349, 225

Buzasi D. L. 1989, PhD Thesis, Pennsylvania State Univ.

Collier Cameron A., 2001, 'Astrotomography - Indirect Imaging Methods in Observational Astronomy', Springer (Lecture Notes in Physics), 183

Chester M. M. 1991, PhD Thesis, Pennsylvania State Univ.

Donati J.-F., Semel M., Carter B., Rees D. E., Collier Cameron A., 1997, MNRAS, 291, 658

Donati J.-F. et al., 2008, MNRAS, 390, 545

Dorren J. D., Guinan E. F., Dewarf L. E., 1994, ASPC, 64, 399

Eggen O. J., 1984a, AJ, 89, 1358

Eggen O. J., 1984b, ApJS, 55, 597

Eggen O. J., 1989, PASP, 101, 366

Elias N. M., II, Dorren J. D., 1990, AJ, 100, 818

Elvis M., Plummer D., Schachter J., Fabbiano G., 1992, ApJS, 80, 257

ESA, 1997, The Hipparcos and Tycho Catalogues, ESA SP-1200

Famaey B., Pont F., Luri X., Udry S., Mayor M., Jorissen A., 2007, A&A, 461, 957

Famaey B., Siebert A., Jorissen A., 2008, A&A, 483, 453

Favata F., Barbera M., Micela G., Sciortino S., 1993, A&A, 277, 428

Fisher R.A., 1935, Design of Experiments, Oliver and Boyd, Edinburgh.

Fisher R.A., 1936, J.R.Anthropol.Inst., 66, 57.

Gálvez M. C. et al., 2002, A&A, 389, 524

Gálvez M. C., 2005, PhD Thesis, Universidad Complutense de Madrid

Gálvez M. C. et al., 2007, A&A, 472, 587

Gálvez M. C. et al., 2009, AJ, 137, 3965

Golovin A., Pavlenko E., Kuznyetsova Y., Krushevska V., 2007, IBVS, 5748, 1

Granzer T., Schüssler M., Caligari P., Strassmeier K. G, 2000, A&A, 355, 1087

Hall J. C., 1996, PASP, 108, 313

Hall J. C., Ramsey L. W., 1992, AJ, 104, 1942

Huovelin J., Saar S. H., 1991, ApJ, 374, 319

Jeffers S. V., Donati J.-F., Collier Cameron A., MNRAS, 375, 567

Johnson H. L., 1966, ARA&A, 4, 193

Johnson D. R. H., Soderblom D. R., 1987, AJ, 93, 864

Kallinger T., Reegen P., Weiss W. W., 2008, A&A, 481, 571

Kazarovets E. V., Samus N. N., Durlevich O. V., Frolov M. S., Antipin S. V., Kireeva N. N., Pastukhova E. N., 1999, IBVS, 4659, 1

Kozhevnikova A. V., Alekseev I. Y., Heckert P. A., Kozhevnikov V. P., 2006, IBVS, 5723, 1

Kupka F., Piskunov N., Ryabchikova T. A., Stempels H. C., Weiss W. W., 1999, A&AS, 138, 119

Kupka F. G., Ryabchikova T. A., Piskunov N. E., Stempels H. C., Weiss W. W., 2000, BaltA, 9, 590

Kurucz R. L. 1993, in Astronomical Society of the Pacific Conference Series, Vol. 44, IAU Colloq. 138: Peculiar versus Normal Phenomena in A-type and Related Stars, ed. Dworetsky M. M., Castelli F., Faraggiana R., 87.

Kuschnig R., Weiss W. W., Gruber R., Bely P. Y., Jenkner H., 1997, A&A, 328, 544

Lenz P., Breger M., 2005, Communications in Asteroseismology, 146, 53

López-Santiago J., Montes D., Fernández-Figueroa M. J., Ramsey L. W., 2003, A&A, 411, 489

López-Santiago J., Micela G., Montes D., 2009, A&A, 499, 129

López-Santiago J., Montes D., Gálvez-Ortiz M. C., Crespo-Chacón I., Martínez-Arnáiz R. M., Fernández-Figueroa M. J., de Castro E., Cornide M., 2010, A&A, 514, A97

Lorente R., Montesinos B., 2005, AJ, 632, 1104

Maldonado J., Martínez-Arnáiz R. M., Eiroa C., Montes D., Montesinos B., 2010, A&A, 521A, 12

Mamajek E. E., Hillenbrand L. A., 2008, ApJ, 687, 1264

Martínez-Arnáiz R., Maldonado J., Montes D., Eiroa C., Montesinos B., 2010, A&A, 520, A79

Martínez Fiorenzano A. F., Gratton R. G., Desidera S., Cosentino R., Endl M., 2005, A&A, 442, 775

Medhi B. J., Maheswar G., Brijesh K., Pandey J. C., Kumar T. S., Sagar R., 2007, MNRAS, 378, 881

Melo C., Pasquini L., de Medeiros J. R. 2004, in IAU Symposium, Vol. 215, Stellar Rotation, ed. Maeder A., Eenens P., 455

Mohanty S., Basri G., 2003, ApJ, 583, 451

Montes D., Fernández-Figueroa M. J., De Castro E. et al., 2000, A&AS, 146, 103

Montes D., López-Santiago J., Gálvez M. C. et al., 2001a, MNRAS, 328, 45

Montes D., López-Santiago J., Fernández-Figueroa M. J., Gálvez M. C., 2001b, A&A, 379, 976

Montgomery M. H., Odonoghue D., 1999, DSSN, 13, 28

Morin J. et al., 2008, MNRAS, 390, 567

Noyes R. W., Hartmann L. W., Baliunas S. L., Duncan D. K., Vaughan A. H., 1984, ApJ, 279, 763

O'Neal D., Saar S. H., Neff J. E., 1996, ApJ, 463, 766

O'Neal, D., Neff, J. E. & Saar, S. H. 1998, ApJ, 507, 919

O'Neal, D., Neff, J. E., Saar, S. H., & Cuntz, M. 2004, AJ, 128, 1802

Pandey J. C., Singh K. P., Sagar R., Drake S. A., 2002, IBVS, 5351, 1

Pandey J. C., 2003, BASI, 31, 329

Pandey J. C., Singh K. P., Drake S. A., Sagar R., 2005, AJ, 130, 1231

Pandey J. C., Medhi B. J., Sagar R., Pandey A. K., 2009, MNRAS, 396, 1004

Panov K., Goranova Y., Genkov V., 2000, IBVS, 4917, 1

Pepper J., Stanek K. Z., Pogge R. W., Latham D. W., DePoy D. L., Siverd R., Poindexter S., Sivakoff G. R., 2008, AJ, 135, 907

Perryman M. A. C. et al., 1997, A&A, 323, L49

Pojmanski G., 2002, AcA, 52, 397

Queloz D., Allain S., Mermilliod J.-C., Bouvier J., Mayor M. 1998, A&A, 335, 183

Queloz D. et al., 2001, A&A, 379, 279

Saar S. H., Huovelin J., 1993, ApJ, 404, 739

Sbordone L., Bonifacio P., Castelli F., Kurucz R. L., 2004, MSAIS, 5, 93

Sbordone L., 2005, Memorie della Societa Astronomica Italiana Supplement, 8, 61

Schachter J. F., Remillard R., Saar S. H., Favata F., Sciortino S., Barbera M., 1996, ApJ, 463, 747

Schmidt G. D., Elston R., Lupie O. L., 1992, AJ, 104, 1563

Schüssler M., Caligari P., Ferriz-Mas A., Solanki S. K., Stix M., 1996, A&A, 314, 503

Tonry J., Davis M., 1979, AJ, 84, 1511

Upgren A. R., Sperauskas J., Boyle R. P., 2002, BaltA, 11, 91

Voges W. et al., 1999, A&A, 349, 389

Zhao J., Zhao G., Chen Y., 2009, ApJ, 692, L113

This paper has been typeset from a TEX/ LATEX file prepared by the author.